Research Article | Vol. 11, No. 10 / 1 October 2020 / Biomedical Optics Express 5760
Biomedical Optics EXPRESS

Single wavelength measurements of absorption coefficients based on iso-pathlength point

IDIT FEDER, HAMOOTAL DUADI, AND DROR FIXLER*

Faculty of Engineering and the Institute of Nanotechnology and Advanced Materials, Bar Ilan University, Ramat Gan 5290002, Israel
Dror.Fixler@biu.ac.il

Abstract: In optical sensing, to reveal the chemical composition of tissues, the main challenge is isolating absorption from scattering. Most techniques use multiple wavelengths, which adds an error due to the optical pathlength differences. We suggest using a unique measurement angle for cylindrical tissues, the iso-pathlength (IPL) point, which depends on tissue geometry only (specifically the effective radius). We present a method for absorption assessment from a single wavelength at multiple measurement angles. The IPL point presented similar optical pathlengths for different tissues, both in simulation and experiments, hence it is optimal. Finally, *in vivo* measurements validated our proposed method.

1. Introduction

Optical sensing in the medical field is rapidly developing in recent years, because it evaluates physiological parameters non-invasively. Imaging of biological tissue is challenging due to the turbidity of the substance, therefore in bio-photonics, the focus is sensing changes in absorption [1].

In material science, the chemical composition of the medium is commonly examined by its interaction with an electromagnetic field. The field is attenuated after interacting with the medium relative to the scattering and absorption [2]. The non-ionizing nature of optical sensing, makes it attractive in the medical field. The microstructure of tissue contributes to the scattering, while the biochemical property is responsible for the absorbance [3]. The reemitted light from tissue is influenced evenly and inseparably by absorption and scattering. Absorption in liquids is measured by spectral measurements in reflection or transmission [4–7]. Solid absorption measurements simplify the geometry and utilize several sources in different wavelengths [8] or different entrance angles [9–11]. These methods assume that the scattering changes between the sources are negligible or can be calibrated [12].

A quantitative value of absorption, from optical methods, is required in order to analyze physiological states. The challenge of extracting this parameter from intensity measurements is the strong dependency on the optical pathlength (OPL), which affects the intensity attenuation as well.

In turbid media, the OPL is larger than the physical distance (d). In order to find the OPL, one must know the differential pathlength factor (DPF). The OPL (l) of the photon [13] is defined by the DPF which is the correction of the physical source-detector distance:

$$l(\mu_a(\lambda), \mu_s'(\lambda)) = DPF(\mu_a(\lambda), \mu_s'(\lambda)) \cdot d \tag{1}$$

where μ_a is the absorption coefficient and μ_s' is the reduced scattering coefficient, both of which depend on the wavelength. Many studies have tried to evaluate the DPF [14–18], using simulation and experiments. Time-resolved experiments were performed to estimate the DPF value of different types of tissues in the range of NIR wavelengths. The time delay of the photons, from picosecond pulse, is evidence of the light propagation distance through the medium. In addition, frequency-domain measurements were performed to approximate the DPF [19]. Reported values

#401591 https://doi.org/10.1364/BOE.401591
Journal © 2020 Received 30 Jun 2020; revised 3 Sep 2020; accepted 3 Sep 2020; published 22 Sep 2020

Biomedical Optics EXPRESS

of the DPF are commonly more than 3, in accordance with wavelength, the medium's absorption, and the detector position (for a distance greater than 2.5 cm the value is stable). The dependency on changes in tissue absorption might cause the DPF to change by 30% [20]. Hence, without taking these influences into account properly, the error for the extracted optical properties is significant.

There are theoretical models for describing the DPF derived from the time-domain solution of the radiative transfer equation (RTE) [21].

For a semi-infinite geometry the DPF is defined as [16]:

$$DPF_{semi} \approx \frac{\sqrt{3\mu_s'}}{2\sqrt{\mu_a}} \frac{d\sqrt{3\mu_s'\mu_a}}{d\sqrt{3\mu_s'\mu_a} + 1}. \tag{2}$$

Hence, the DPF is different for each wavelength, and the ratiometric measurements of tissues, which contained nonhomogeneous layers, suffered from an inherent error.

In contrast to the previous methods, our research shows that if the geometry is taken into account, self-calibration measurements can be done, using a point that is invariant to the scattering. This self-calibration point, i.e. the iso-pathlength (IPL) point, depends on the position in accordance with the geometry only. At this point, the OPL is stable under changes in medium structure and allows an absolute, and not relative, absorption measurement.

Tissue oxygenation is commonly assessed by an absorption measurement from cylindrical tissues, such as a human finger, lip, and earlobe [22–24]. This geometry enables a unique optical characterization, not only by reflection or transmission of light. The full scattering profile (FSP), which means the light intensity distribution on the generatrix of a cylinder (Fig. 1) surface where $0° < \theta < 360°$, is easily measurable for this geometry. Using the FSP the IPL point is revealed.

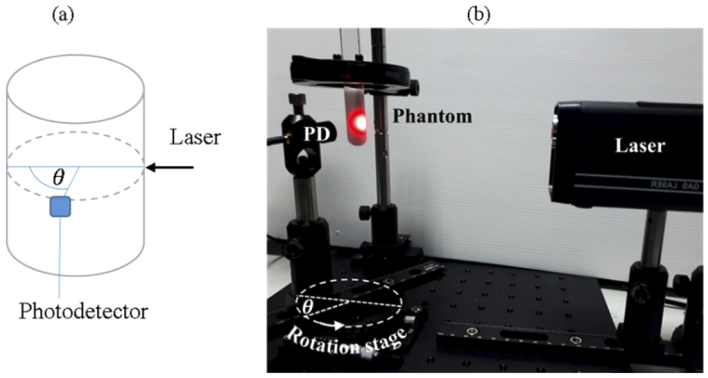

Fig. 1. (a) FSP of cylindrical geometry is the light distribution on the cylinder circumference (on the dashed line) from $\theta = 0°$ to $\theta = 360°$. (b) The experimental setup for measuring the FSP: A single wavelength measurement at multiple angles from a cylindrical sample.

In this research, we present for the first time a method for extracting the absorption coefficient by a single wavelength, using the IPL point. It will add accuracy in contrast to the errors with the ratiometric analysis of multiwavelength systems. First, we will show that at the IPL point the OPL is constant. The OPL, which is longer than the physical distance, is described by the DPF. Hence, the DPF at the IPL point in the case of no absorption will be presented. Next, we will present a method for describing the shortening of the DPF in the presence of absorption. Since the absorption is unknown, we suggest assessing this parameter through the decrease in intensity. Thus, we will show a method for calculating absorption according to the intensity and knowledge of the position of the IPL point.

Biomedical Optics EXPRESS

In addition, we developed an equation for extracting the absorption coefficient from the intensity at the IPL point. Next, a unique experimental system is used to measure tissue-like phantoms. The system measures the light intensities of different scattering substances without absorption in comparison to the phantoms with different absorption coefficients. Based on the suggested equation, the absorption was extracted from the measured phantoms using a single wavelength. Finally, the optical measurement of the index finger (human) confirms our proposed method. The values measured *in vivo* correspond to known tissue values in literature.

2. Theory

Absorption theory originates from the Beer-Lambert law [25]. This theorem describes the influence of the absorption coefficient, μ_a, on the intensity of light, I_t, after passing through a medium. In its original form, the Beer-Lambert law is applicable in a non-scattering condition, where the intensity decreases exponentially according to the sample thickness. However, for turbid media, the modified Beer-Lambert law (MBLL) is more suitable:

$$I_t = I_{in}\exp(-\mu_a l - G) \tag{3}$$

where I_{in} is the input illumination, G is a geometry-dependent factor which describes the attenuation due to scattering and location in a specific geometry, and l represents the OPL. We define the light intensity without absorption $I_0=I_{in}\exp(-G)$. The optical properties as well as the OPL depend on the wavelength of the irradiated light.

In the case of a cylindrical-shaped tissue, the intensity distribution as a function of the exit angle, θ, (Fig. 1) for a given wavelength is:

$$I_t(\theta, \mu_a, \mu_s') = I_0(\theta, \mu_s')\exp[-\mu_a \cdot l(\theta, \mu_a, \mu_s')]. \tag{4}$$

This equation depends on the measurement position as well as the optical properties of the media. Therefore, the ratiometric measurements using two wavelengths add an unavoidable error without considering the change of OPL as a function of wavelength [26–28].

We found that an angle exists, i.e. the iso-pathlength (IPL) point, where the light intensity does not depend on scattering [29–32]. Meaning that the OPL is constant for different scattering coefficients. This phenomenon makes the IPL point optimal for extracting the absorption coefficient, assuming that the OPL at this point is known.

At the IPL point, the OPL does not depend on the scattering, and the intensity is constant. Hence, Eq. (4) becomes:

$$I_t(\theta_{IPL}, \mu_a) = I_0(\theta_{IPL})\exp[-\mu_a \cdot d \cdot DPF(\mu_a)] \tag{5}$$

where physical distance, d, is defined for a cylinder with a diameter D:

$$d = D \cdot \sin\left[\frac{180 - \theta_{IPL}}{2}\right]. \tag{6}$$

Taking the natural logarithm on Eq. (5) and using Eq. (6) we derive:

$$\mu_a = \frac{\ln[I_t(\theta_{IPL})/I_0(\theta_{IPL})]}{D \cdot \sin\left[\frac{180-\theta_{IPL}}{2}\right] \cdot DPF} \tag{7}$$

where the I_0 is measured using phantoms without absorption, and the DPF expression is calculated from phantom measurements with scattering and absorption properties, as described below in **section 3c** Eq. (11). By Eq. (7), the absorption coefficient is extracted with a single wavelength.

Biomedical Optics EXPRESS

3. Materials and methods

3.1. Optical system

Our set-up includes a CW He-Ne laser with a wavelength of 632.8nm, and 0.8mW power (Thorlabs, Japan). This laser is used to illuminate cylindrical samples (phantoms or fingers). The full scattering profile is collected using a photodiode (PD) with an active area of 13mm^2. The PD is placed on a rotation stage and connected to an amplification circuit (Fig. 1). The light intensity is measured every 5-degrees, from the transmission light (zero degrees) to the source direction, until 150 degrees.

3.2. Solid tissue-like phantom preparation

The phantom contains Intra Lipid (IL, IntraLipid 20% Emulsion, Sigma-Aldrich, Israel) as a scattering component, Ink (Indian ink 1%) as an absorbent, and 1% agarose powder (SeaKem LE Agarose, Ornat, Israel) for solidification. The solution was prepared in two separate steps which were mixed at the end of the process. The first part contains 2% agarose powder melted in double-distilled water (slowly added at ~70°C temperature). The second part includes the intra-lipid and ink in various concertation diluted in double-distilled water. After mixing the two parts, the final solution was poured into glass tubes in different diameters (10mm and 13mm).

First, phantoms with varying IL concentrations but without Ink were prepared. These phantoms are used to find the IPL point and measure I_0 from Eq. (4). Next, phantoms with varying IL and Ink concentrations were prepared. The absorption coefficient was measured by solutions with the different ink concentrations without IL and agarose. These solutions were measured using a UV-VIS spectrophotometer (Shimadzu, UV-1900, Japan) to verify the absorption coefficients (at the bottom of Table 1) before the preparation of the solid phantoms. The measured absorption coefficient matched the expected values [33].

Table 1. The concentration of IL and Ink in solid phantoms

Scattering coefficient (cm^{-1})	**IL concentration (10^{-2})**
16	2
20	2.5
26	3.25
Absorption coefficient (cm^{-1})	**Ink concentration (10^{-5})**
0.13	2.2
0.25	4.4
0.37	6.4
0.48	8.4

The optical parameters were chosen in accordance with the human fingers' range of scattering as well as absorption. In the absorption values, we used oxy and deoxy-hemoglobin absorption parameters in a wavelength of 633nm, including the fact that the blood volume is 5% of the finger volume [34]. In the range of different blood oxygen saturation, we calculate the relevant absorption coefficients for our study.

3.3. Monte Carlo simulation

The simulation describes the FSP of a cylindrical tissue at all exit angles based on the Monte-Carlo (MC) method [35]. For each step (r), the probability of a photon to be absorbed (p_a), or scattered (p_s), depends on μ_a and μ'_s, as follows:

$$p_a = 1 - \exp(-\mu_a r) \tag{8}$$

$$p_s = 1 - \exp(-\mu_s r). \tag{9}$$

Biomedical Optics EXPRESS

If the photon is scattered, its new direction is calculated according to:

$$\theta_{new} = \theta_{old} + s \cdot \cos^{-1}(g) \tag{10}$$

where g is the anisotropy factor and s is a random number from the group {−1, 1} [7]. The simulation repeats the calculations until the photon exits the tissue. The OPL of each photon and its output position are collected. In the end, the average OPL was calculated. In addition, the DPF was extracted according to the OPL, depending on the physical distance from the light source. The simulation was performed for different scattering coefficients, absorption coefficients, and tissue diameters.

4. Results

4.1. IPL point for calibrating the OPL

The FSPs of cylindrical phantoms with no absorption and different reduced scattering coefficients were measured in the optical system [results of 13mm diameter phantom in Fig. 2(a)]. The direction of photons that did not experience scattering is described as zero degrees and the laser position is described as 180 degrees [inset of Fig. 2(a)]. The common point between the curves is the IPL point, which appears at 120 degrees [Fig. 2(b)]. At this point, the light intensity does not depend on the presence of scattering components. As we reported in a previous study [29], there is a linear dependency between the position of the IPL point and the tissue diameter. Hence, this specific angle (120 degrees) is relevant for phantoms with a specific diameter (13mm).

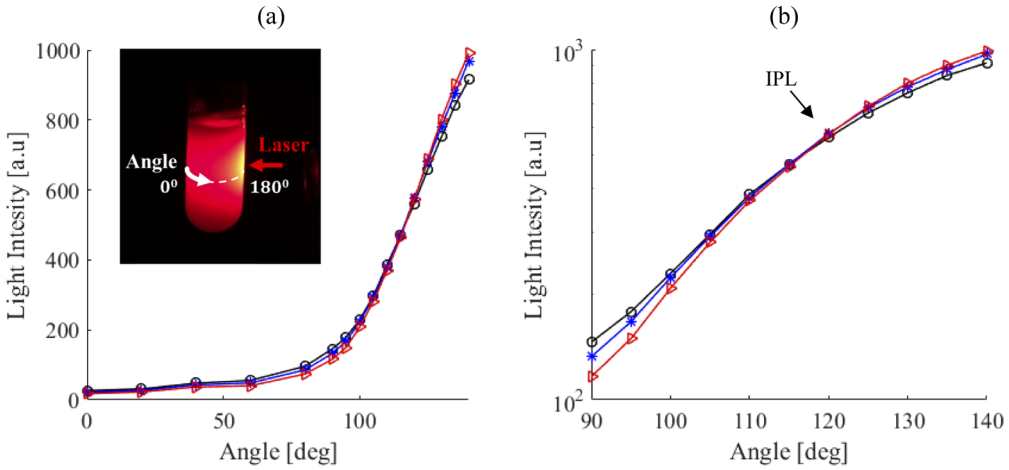

Fig. 2. (a) FSP of phantoms with different scattering coefficients (black circles, blue asterisks and red triangles represent 16 cm^{-1}, 20 cm^{-1}, 26 cm^{-1} respectively). Inset: The laser position is defined as 180 degrees, and full transmission as zero degrees. (b) Enlargement of the FSPs in logarithmic scale. The black arrow marks the position of the IPL point.

4.2. Influence of absorption on the IPL point

In order to examine the influence of absorption on the full scattering profile, phantoms with the same diameter and scattering coefficient with different absorption coefficients were measured (results of 10mm diameter phantom in Fig. 3). The FSP shapes are similar, while the intensity decreases as the absorption is higher.

The intensity for each absorption value can be described according to Eq. (4) as a function of the intensity without absorption, the absorption coefficient and the optical pathlength. Since we

Biomedical Optics EXPRESS

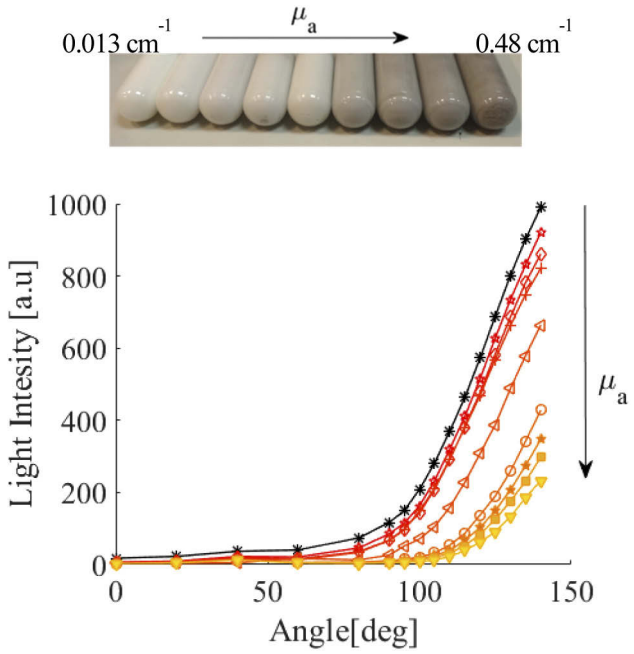

Fig. 3. The influence of absorption at a given scattering of 20 cm^{-1} and 10 mm diameter. Full scattering profile of phantoms without absorption (black star), and with absorption of 0.013 cm^{-1} (stars), 0.025 cm^{-1} (diamonds), 0.036 cm^{-1} (plus), 0.048 cm^{-1} (triangles), 0.13 cm^{-1}(circles), 0.25 cm^{-1} (full stars), 0.36cm^{-1} (full squares) and 0.48 cm^{-1} (full triangles) decays respectively. Inset: Image of phantoms with constant scattering and diameter and increasing absorption, measured in the graphs.

know the physical distance in the measurement position, with the purpose of finding the OPL, the DPF is needed.

4.3. DPF in the presence of absorption

A MC simulation was performed in order to examine the OPL and the DPF accordingly, in the case of cylindrical media. First, we examined the case of no absorption. The OPL is longer than the distance from the source [Fig. 4(a) for a scattering coefficient of 20cm^{-1}].

The MC simulation calculates the OPL, and then the DPF as a function of the distance from the source was computed according to Eq. (1) [Fig. 4(b)]. The pattern of these graphs is in accordance with the report of Chatterjee et al. that used MC simulation for higher wavelength [14]. There, the DPF of 660nm and 880nm showed an increase and then linear decrease, with a maximum at around 4 mm. The maximum DPF value for 880nm is 5.5 and for 660nm is 7.5. Hence, the maximum DPF value of 18 found in our simulation for a lower wavelength matches this trend. For a distance of 6mm, corresponding to the IPL point, the DPF of no absorption was found to be DPF_0=12. This value will be used in the experimental section. This value can be received from Eq. (2) by placing μ'_s=20cm^{-1} and μ_a=0.01cm^{-1}, which is the minimal absorption of our phantoms (caused by water and IL).

Based on the simulation results, the DPF shortening in the presence of absorption is examined (Fig. 5). The DPF changes with absorption are in accordance with the literature [20].

We conclude the DPF shortening in case of absorption, as detailed in Supplement 1:

$$DPF = DPF_0 \cdot \sqrt{R} \tag{11}$$

Biomedical Optics EXPRESS

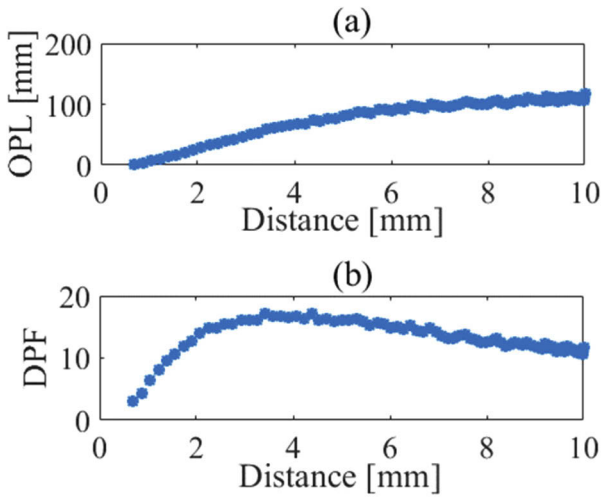

Fig. 4. Simulation results of the (a) OPL and the (b) DPF as a function of the distance from the light source in a cylindrical tissue with a scattering coefficient of 20cm^{-1} and a diameter of 10 mm.

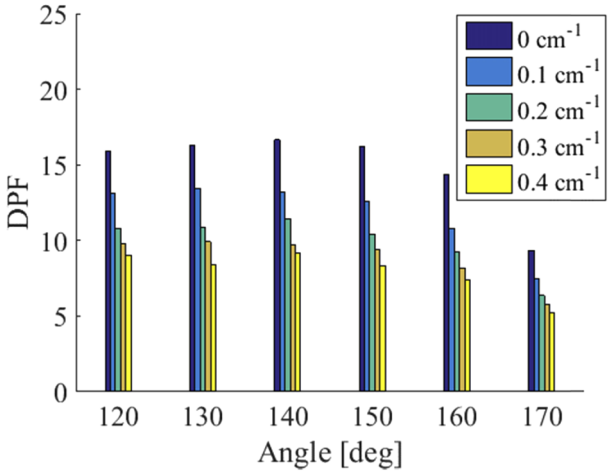

Fig. 5. DPF shortening in the presence of absorption. The DPF for different absorptions (0, 0.1, 0.2, 0.3, and 0.4 cm^{-1}) as a function of angle.

Biomedical Optics EXPRESS

where R is the ratio between the intensities at the IPL point with absorption (I_t) and without absorption (I_0):

$$R = \frac{I_t(\theta_{IPL})}{I_0(\theta_{IPL})} \tag{12}$$

Equation (11) was critical for our method. As we mentioned above, the OPL shortens as a function of the absorption coefficient (Eq. (2)). However, since we are interested in extracting the absorption coefficient, we must find a way to represent the DPF shortening from the decrease in the intensity. In the next section, the experimental results will prove Eq. (11).

In order to extract the absorption coefficients from experiment results, we used Eqs. (7), (11) and (12):

$$\mu_a = -\frac{1}{DPF_0\sqrt{R}\cdot D\cdot \sin\left(\frac{180-\theta_{IPL}}{2}\right)}\ln(R). \tag{13}$$

In this equation, we used the diameter of the phantom, which is easily measured. In addition, the DPF_0 value, from the simulation, for correcting the distance for the practical OPL. Finally, the absorption is extracted by the light intensity in the IPL point.

4.4. Extraction of the absorption coefficient

4.4.1. Phantoms

Solid phantoms with different scattering coefficients and different absorption coefficients were prepared in order to measure the absorption. The FSP of these phantoms was measured in our unique optical system (Fig. 1). The IPL point appeared at the same angle for the profiles of the phantoms without absorption (black circles in Fig. 6) and for the profiles of the phantoms with absorption (red stars in Fig. 6). The light intensity at the IPL point without absorption ($I_0(\theta_{IPL})$) is higher than the intensity at the IPL point with absorption ($I_\mu(\theta_{IPL})$). These values are used to calculate R (Eq. (12)), and the absorption coefficient is calculated from Eq. (13) given the DPF_0 value measured previously (**section 3c**).

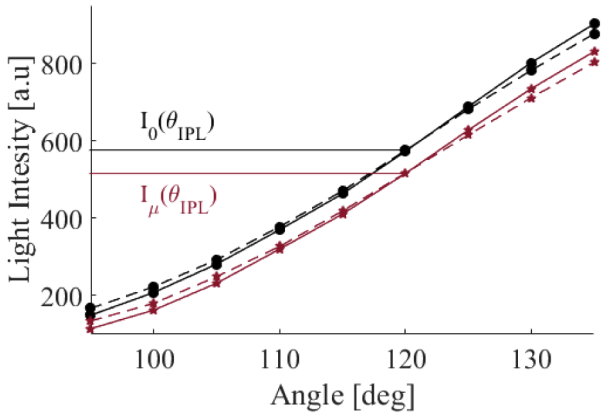

Fig. 6. Experimental full scattering profiles of phantoms without absorption (circles) in comparison to phantoms with absorption (0.13cm^{-1}, stars). Both are 13 mm diameter with the same scattering components. The solid line corresponds to the scattering coefficient of 20cm^{-1} and the dashed line corresponds to 26cm^{-1}. In this work, we presented a method for extracting the absorption coefficient using one wavelength.

The absorption values of phantoms with different absorptions in two different diameters were calculated in this manner (Fig. 7). The results are in accordance with the known absorption values from the preparation section, even absorptions of under 0.05cm^{-1}.

Biomedical Optics EXPRESS

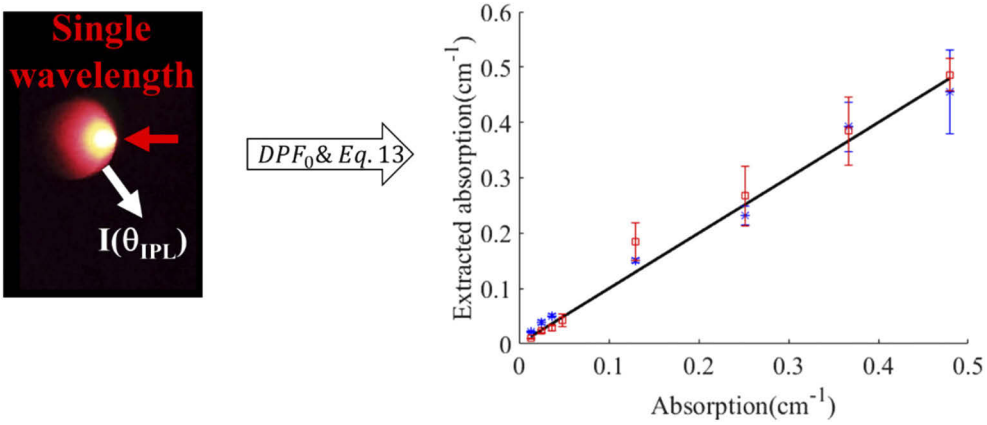

Fig. 7. Extracted absorption coefficient from phantom measurements according to Eq. (13) (dots) in comparison to the known absorption coefficients (line) with different diameters: 10 mm (blue asterisks) and 13 mm (red squares), based on the IPL point at 105 degrees and 120 degrees respectively.

4.4.2. *In vivo* measurements

To validate our proposed method, we measured the optical parameters of the index finger. Measurements were performed on three volunteers (women) with different skin tones in the optical system. The position of the IPL point was determined in accordance with the effective diameter of the fingers, as the finger is more an ellipse [36]. The average effective diameter of the fingers is 11.7 cm. The inner (palm) side of the finger was irradiated, as shown in Fig. 8, since the difference between the skin tones is smaller. Based on our method, the light intensity of the IPL point was compared to the control phantoms without absorption, in the appropriate diameter. Using the single wavelength measurement and the DPF as in the preliminary experiment, the finger absorption results (Fig. 8(b)) are in accordance with the literature [37]. Note that the error of the measurements stems from a 5 degree displacement of the system.

(a)

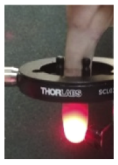

(b)

sample	Absorption coefficient (cm^{-1})
1	0.482±0.018
2	0.477±0.018
3	0.477±0.018

Fig. 8. (a) A finger absorption coefficient measurement, using a single wavelength. (b) Extracted absorption coefficients of fingers.

5. Discussion and conclusion

In this work, we presented a method to extract the absorption coefficient using one wavelength from cylindrical tissues based on the FSP of the tissue. We presented the optical system for measuring the light distribution by a photodetector and a red laser. Experimental results of FSPs for cylindrical phantoms with various reduced scattering coefficients reveal an IPL point, where the OPL depends on the geometry and not on the scattering. The light intensity at all exit angles except for the IPL point is influenced by both scattering and absorption. Hence, in order to

Biomedical Optics EXPRESS

neutralize the scattering influence, the IPL is the optimal measurement position. Solid phantoms with absorptions in the range of 0.013cm^{-1} - 0.48cm^{-1} have shown an intensity attenuation of the FSP, while the trend of the profile remains the same. Assessment of the absorption coefficient from this intensity decrease requires the OPL, which decreases with absorption as well. We propose describing this change by the square root of the intensity attenuation in the IPL point, since the absorption coefficient is unknown. For the case of no absorption, we presented the DPF value of 12 in the IPL point using the MC simulation, supported by theoretical calculation. Examining phantoms with and without absorption, revealed the same IPL point, in accordance with the tissue geometry, for phantoms with 10mm and 13mm diameter. The IPL point, in different diameters, is in a similar distance to the light source, hence the DPF value of 12 is relevant for the different diameters. We showed that the results of our proposed method fit well with the preparation properties of the absorption coefficient in phantoms with different diameters. The accuracy of the measurement system is 5 degrees due to the rotation stage accuracy, hence the error in the position of the IPL point is in this range, and the extraction error is calculated respectively. The accuracy in the absorption coefficient using our method due to a 5-degree error in the IPL position is 0.018cm^{-1} corresponding to 1.5% error in blood oxygen saturation. In addition, we presented *in vivo* measurements of human fingers in the optical system, using our method. The absorption coefficients extracted by our method were in good agreement with literature reports. The dynamic range of absorption coefficients used in our experiments is relevant to the range of human tissue [38,39]. Our ability to distinguish different μ_a values, with high precision, is very important for noninvasive sensing. The limitation of the light intensity distribution measurements is close to the light source where the detector blocks the laser (angles higher than 150°). Following our simulation results that simulated the high exit angles, the light intensity above the IPL point is not needed for our extraction method. Therefore, the experimental system limitation, of the high angles measurements, does not affect the method, since the light intensity can still be measured at the IPL point and its surroundings.

The new point of view of the FSP produces a novel characterization of tissues using a single wavelength. The extraction of absorption in a single wavelength overcomes the calibration process needed in methods based on several wavelengths. Hence, the personalized data with specific analysis is more accurate. It can support early detection of exposure to the COVID-19 virus where some infected patients who have very low blood oxygen saturation levels and are not even aware of the lack of oxygenation in their bodies. Moreover, the use of the natural phenomenon of the IPL point, which also exists in other geometries [32,40], such as a semi-infinite geometry, can be relevant for a wide range of NIR measurements in the biomedical sensing field. For example, sensing of physiological states and metabolism processes associated with oxygen concentration in breast and head tissues.

Funding

Israel Science Foundation (ISF) (1195/18).

Disclosures

The authors declare no conflicts of interest.

See Supplement 1 for supporting content.

References

1. F. F. Jobsis, "Noninvasive, infrared monitoring of cerebral and myocardial oxygen sufficiency and circulatory parameters," Science **198**(4323), 1264–1267 (1977).

Biomedical Optics EXPRESS

2. A. Roggan, M. Friebel, K. Dörschel, A. Hahn, and G. J. Mueller, "Optical properties of circulating human blood in the wavelength range 400-2500 nm," J. Biomed. Opt. **4**(1), 36–47 (1999).
3. J. R. Mourant, T. Fuselier, J. Boyer, T. M. Johnson, and I. J. Bigio, "Predictions and measurements of scattering and absorption over broad wavelength ranges in tissue phantoms," Appl. Opt. **36**(4), 949–957 (1997).
4. J. W. Pickering, S. A. Prahl, N. Van Wieringen, J. F. Beek, H. J. Sterenborg, and M. J. Van Gemert, "Double-integrating-sphere system for measuring the optical properties of tissue," Appl. Opt. **32**(4), 399–410 (1993).
5. S. Fantini, M. A. Franceschini, J. B. Fishkin, B. Barbieri, and E. Gratton, "Quantitative determination of the absorption spectra of chromophores in strongly scattering media: a light-emitting-diode based technique," Appl. Opt. **33**(22), 5204–5213 (1994).
6. B. W. Pogue and M. S. Patterson, "Frequency-domain optical absorption spectroscopy of finite tissue volumes using diffusion theory," Phys. Med. Biol. **39**(7), 1157–1180 (1994).
7. A. Kienle, L. Lilge, M. S. Patterson, R. Hibst, R. Steiner, and B. C. Wilson, "Spatially resolved absolute diffuse reflectance measurements for noninvasive determination of the optical scattering and absorption coefficients of biological tissue," Appl. Opt. **35**(13), 2304–2314 (1996).
8. M. Nitzan, S. Noach, E. Tobal, Y. Adar, Y. Miller, E. Shalom, and S. Engelberg, "Calibration-free pulse oximetry based on two wavelengths in the infrared—A preliminary study," Sensors **14**(4), 7420–7434 (2014).
9. Y. Mendelson, A. C. Clermont, R. A. Peura, and B.-C. Lin, "Blood glucose measurement by multiple attenuated total reflection and infrared absorption spectroscopy," IEEE Trans. Biomed. Eng. **37**(5), 458–465 (1990).
10. D. Roessler and F. Faxvog, "Optoacoustic measurement of optical absorption in acetylene smoke," J. Opt. Soc. Am. **69**(12), 1699–1704 (1979).
11. I. Šimon, "Spectroscopy in infrared by reflection and its use for highly absorbing substances," J. Opt. Soc. Am. **41**(5), 336–345 (1951).
12. J. S. Dam, P. E. Andersen, T. Dalgaard, and P. E. Fabricius, "Determination of tissue optical properties from diffuse reflectance profiles by multivariate calibration," Appl. Opt. **37**(4), 772–778 (1998).
13. M. Bhatt, K. R. Ayyalasomayajula, and P. K. Yalavarthy, "Generalized Beer–Lambert model for near-infrared light propagation in thick biological tissues," J. Biomed. Opt. **21**(7), 076012 (2016).
14. S. Chatterjee, T. Y. Abay, J. P. Phillips, and P. A. Kyriacou, "Investigating optical path and differential pathlength factor in reflectance photoplethysmography for the assessment of perfusion," J. Biomed. Opt. **23**(07), 1 (2018).
15. D. T. Delpy, M. Cope, P. van der Zee, S. Arridge, S. Wray, and J. Wyatt, "Estimation of optical pathlength through tissue from direct time of flight measurement," Phys. Med. Biol. **33**(12), 1433–1442 (1988).
16. S. Fantini, M. A. Franceschini, E. Gratton, D. Hueber, W. Rosenfeld, D. Maulik, P. G. Stubblefield, and M. R. Stankovic, "Non-invasive optical mapping of the piglet brain in real time," Opt. Express **4**(8), 308–314 (1999).
17. M. A. Kamran, M. Mannann, and M. Y. Jeong, "Differential Path-Length Factor's Effect on the Characterization of Brain's Hemodynamic Response Function: A Functional Near-Infrared Study," Front. Neuroinform. **12**, 37 (2018).
18. M. Kohl, C. Nolte, H. R. Heekeren, S. Horst, U. Scholz, H. Obrig, U. Scholz, H. Obrig, and A. Villringer, "Determination of the wavelength dependence of the differential pathlength factor from near-infrared pulse signals," Phys. Med. Biol. **43**(6), 1771–1782 (1998).
19. J. R. Lakowicz and K. Berndt, "Frequency-domain measurements of photon migration in tissues," Chem. Phys. Lett. **166**(3), 246–252 (1990).
20. P. Van der Zee, S. Arridge, M. Cope, and D. Delpy, "The effect of optode positioning on optical pathlength in near infrared spectroscopy of brain," in *Oxygen Transport to Tissue XII*, ed: Springer, 1990, pp. 79–84.
21. S. R. Arridge, M. Cope, and D. Delpy, "The theoretical basis for the determination of optical pathlengths in tissue: temporal and frequency analysis," Phys. Med. Biol. **37**(7), 1531–1560 (1992).
22. H. Komatsu, M. Ikawa, K. Karita, and S. Fukumoto, "Measurement of Tissue Oxygenation Level in Human Lip," in *Interface Oral Health Science 2011*, ed: Springer, 2012, pp. 128–130.
23. K. Akons, E. J. Dann, and D. Yelin, "Measuring blood oxygen saturation along a capillary vessel in human," Biomed. Opt. Express **8**(11), 5342–5348 (2017).
24. I. Yoshiya, Y. Shimada, and K. Tanaka, "Spectrophotometric monitoring of arterial oxygen saturation in the fingertip," Med. Biol. Eng. Comput. **18**(1), 27–32 (1980).
25. R. V. Maikala, "Modified Beer's Law–historical perspectives and relevance in near-infrared monitoring of optical properties of human tissue," Int. J. Ind. Ergon. **40**(2), 125–134 (2010).
26. M. Nitzan, A. Babchenko, B. Khanokh, and H. Taitelbaum, "Measurement of oxygen saturation in venous blood by dynamic near infrared spectroscopy," J. Biomed. Opt. **5**(2), 155–162 (2000).
27. A. Cohen and N. Wadsworth, "A light emitting diode skin reflectance oximeter," Med. Biol. Eng. **10**(3), 385–391 (1972).
28. M. Nitzan, A. Romem, and R. Koppel, "Pulse oximetry: fundamentals and technology update," Medical Devices **7**, 231 (2014).
29. H. Duadi, I. Feder, and D. Fixler, "Linear dependency of full scattering profile isobaric point on tissue diameter," J. Biomed. Opt. **19**(2), 026007 (2014).
30. I. Feder, H. Duadi, and D. Fixler, "Experimental system for measuring the full scattering profile of circular phantoms," Biomed. Opt. Express **6**(8), 2877–2886 (2015).

Biomedical Optics EXPRESS

31. H. Duadi, D. Piao, and D. Fixler, "Calibration iso-pathlength point in cylindrical tissue geometry: comparing steady state photon diffusion to Monte Carlo simulation," in *Nanoscale Imaging, Sensing, and Actuation for Biomedical Applications XVI*, 2019, p. 108911D.
32. I. Feder, H. Duadi, R. Chakraborty, and D. Fixler, "Self-Calibration Phenomenon for Near-Infrared Clinical Measurements: Theory, Simulation, and Experiments," ACS Omega **3**(3), 2837–2844 (2018).
33. R. Cubeddu, A. Pifferi, P. Taroni, A. Torricelli, and G. Valentini, "A solid tissue phantom for photon migration studies," Phys. Med. Biol. **42**(10), 1971–1979 (1997).
34. S. L. Jacques, "Optical assessment of cutaneous blood volume depends on the vessel size distribution: a computer simulation study," J. Biophotonics **3**(1-2), 75–81 (2009).
35. H. Duadi, D. Fixler, and R. Popovtzer, "Dependence of light scattering profile in tissue on blood vessel diameter and distribution: a computer simulation study," J. Biomed. Opt. **18**(11), 111408 (2013).
36. H. Duadi, I. Feder, and D. Fixler, "Near-infrared human finger measurements based on self-calibration point: Simulation and in vivo experiments," J. Biophotonics **11**(4), e201700208 (2018).
37. J. Xiao, L. Yao, Y. Sun, E. S. Sobel, J. He, and H. Jiang, "Quantitative two-dimensional photoacoustic tomography of osteoarthritis in the finger joints," Opt. Express **18**(14), 14359–14365 (2010).
38. S. L. Jacques, "Optical properties of biological tissues: a review," Phys. Med. Biol. **58**(11), R37–R61 (2013).
39. Y. Beiderman, A. D. Amsel, Y. Tzadka, D. Fixler, V. Mico, J. Garcia, M. Teicher, and Z. Zalevsky, "A microscope configuration for nanometer 3-D movement monitoring accuracy," Micron **42**(4), 366–375 (2011).
40. N. Zurgil, Y. Shafran, D. Fixler, and M. Deutsch, "Analysis of early apoptotic events in individual cells by fluorescence intensity and polarization measurements," Biochem. Biophys. Res. Commun. **290**(5), 1573–1582 (2002).